Reproducibility assessment of a biomechanical model-based elasticity imaging method for identifying changes in left ventricular mechanical stiffness

Caroline E. Miller[a,b] **Jennifer H. Jordan**[c] **Emily Douglas**[d] **Katherine Ansley**[d] **Alexandra Thomas**[d,e] **and Jared A. Weis**[a,b,e,*]

[a]Wake Forest School of Medicine, Biomedical Engineering, Winston-Salem, North Carolina, United States

[b]Virginia Tech-Wake Forest University, School of Biomedical Engineering and Sciences, Blacksburg, Virginia, United States

[c]Virginia Commonwealth University, Biomedical Engineering and Pauley Heart Center, Richmond, Virginia, United States

[d]Atrium Health Wake Forest Baptist, Hematology and Oncology, Winston-Salem, North Carolina, United States

[e]Atrium Health Wake Forest Baptist, Comprehensive Cancer Center, Winston-Salem, North Carolina, United States

Abstract

Purpose: Cardiotoxicity of antineoplastic therapies is increasingly a risk to cancer patients treated with curative intent with years of life to protect. Studies highlight the importance of identifying early cardiac decline in cancer patients undergoing cardiotoxic therapies. Accurate tools to study this are a critical clinical need. Current and emerging methods for assessing cardiotoxicity are too coarse for identifying preclinical cardiac degradation or too cumbersome for clinical implementation.

Approach: In the previous work, we developed a noninvasive biomechanical model-based elasticity imaging methodology (BEIM) to assess mechanical stiffness changes of the left ventricle (LV) based on routine cine cardiac magnetic resonance (CMR) images. We examine this methodology to assess methodological reproducibility. We assessed a cohort of 10 participants that underwent test/retest short-axis CMR imaging at baseline and follow-up sessions as part of a previous publicly available study. We compare test images to retest images acquired within the same session to assess within-session reproducibility. We also compare test and retest images acquired at the baseline imaging session to test and retest images acquired at the follow-up imaging session to assess between-session reproducibility.

Results: We establish the within-session and between-session reproducibility of our method, with global elasticity demonstrating repeatability within a range previously demonstrated in cardiac strain imaging studies. We demonstrate increased repeatability of global elasticity compared to segmental elasticity for both within-session and between-session. Within-subject coefficients of variation for within-session test/retest images globally for all modulus directions and a mechanical fractional mechanical stiffness anisotropy metric ranged from 11% to 28%.

Conclusions: Results suggest that our methodology can reproducibly generate estimates of relative mechanical elasticity of the LV and provides a threshold for distinguishing true changes in myocardial mechanical stiffness from experimental variation. BEIM has applications in identifying preclinical cardiotoxicity in breast cancer patients undergoing antineoplastic therapies.

 [DOI: 10.1117/1.JMI.9.5.056001]

Keywords: biomechanical modeling; magnetic resonance imaging; reproducibility; cardiac; elasticity; cardiotoxicity.

*Address all correspondence to Jared A. Weis, jweis@wakehealth.edu

Paper 22044GRR received Feb. 17, 2022; accepted for publication Oct. 4, 2022; published online Oct. 22, 2022.

1 Introduction

Cardiac disease is the leading cause of death in the United States.[1] Cardiac disease encompasses many different pathologies, but changes in myocardial stiffness preceding irreversible disease are a common occurrence. Recent studies underscore the importance of identifying early biomarkers for detecting subclinical cardiac disease, particularly for cardiotoxicities that cause irreversible cardiac decline. Treatment-induced cardiotoxicity occurs in up to one quarter of cancer patients worldwide resulting in a large population of cancer patients with treatment dose-limits or long-term cardiac health declines that threaten to undermine considerable survival gains.[2] Antineoplastic therapies are a common cause of cardiotoxicity. This is of particular importance, as this can be dose-limiting and pose a risk for late oncologic events, as well as long-term cardiac damage. In particular, breast cancer therapeutics are associated with an increased risk of cardiovascular events during treatment,[3–5] with evidence suggesting early mitigation of these risks could have more favorable impacts on overall survival than completion of therapeutic regimens.[6] Cardiotoxicity due to breast cancer therapeutics can be characterized by a cardiac remodeling response, in which cardiac fibroblasts deposit an increased level of extracellular matrix (ECM) structural proteins. Extensive cardiac ECM remodeling leads to the formation of fibrotic tissue that infiltrates healthy myocardium, increases myocardial stiffness, and impairs cardiac function. Current global measurements of cardiac dysfunction aim to diagnose cardiotoxicity, but studies indicate significant functional decline is insensitive to early, regional changes in cardiac dysfunction caused by fibrotic infiltration, and is only able to identify functional changes after irreversible cardiac damage has occurred.[7,8] There is a significant need for new noninvasive clinical strategies for identifying subclinical cardiac degradation in patients undergoing antineoplastic therapy for breast cancer. Myocardial tissue stiffness changes may represent a valuable biomarker for cardiac fibrosis to indicate early subclinical cardiac degradation before irreversible damage from breast cancer therapeutics leads to life-threatening cardiac disease.

Current noninvasive imaging methods that are sensitive to changes in myocardial stiffness include ultrasound or magnetic resonance cardiac strain imaging, which involve analyzing gradients of left ventricle (LV) wall deformation as a surrogate of LV mechanical elasticity. As elasticity is equal to the ratio of stress and strain, strain imaging relies on a potentially problematic assumption of a uniform mechanical stress field within the LV wall for assumptions about LV mechanical stiffness properties.[9,10] Ventricular elasticity assumptions through strain imaging are also confounded by changes in size and shape of the ventricle, a common occurrence with cardiotoxicity. To obtain a more direct functional measurement of mechanical elasticity, elastography imaging techniques have been developed to estimate regional mechanical stiffness properties. Elastography methods typically involve mechanical excitation of a tissue of interest resulting in shear wave propagation. Shear wave speed calculated using ultrasound shear wave imaging or displacement images obtained through MR motion encoded gradients are then used within an inverse mechanical elasticity framework to estimate regional elasticity. The resulting elasticity maps are more sensitive to changes in true mechanical stiffness than strain imaging.[10] However, traditional elastography methods are technically challenged for cardiac applications due to complicated inversion calculations and difficulty of producing sufficient shear wave propagation due to complex cardiac structure and inherent LV motion. To address limitations with current and emerging techniques for assessment of cardiac mechanical stiffness, we previously developed a biomechanical model-based elasticity imaging method (BEIM) for estimating direct, functional mechanical stiffness of the LV for the purpose of assessing changes in LV stiffness to identify subclinical cardiotoxicity. BEIM utilizes routinely acquired cine cardiac magnetic resonance (CMR) images to estimate regional mechanical elasticity of the LV based

on observed deformation of the LV interpreted via an inverse computational biomechanics modeling framework. In a previous proof-of-concept correlative imaging study utilizing routine cardiac MR images, we demonstrated LV elasticity differences between cohorts of premenopausal breast cancer patients either undergoing ovarian function suppression concurrent with aromatase inhibitor administration for hormone receptor positive breast cancer or after completion of therapy for triple negative breast cancer.[11]

To further interrogate BEIM, in this study we perform a reproducibility analysis for LV mechanical elasticity measures using publicly available cardiac MR images acquired in a previous study for reproducibility assessment of myocardial radiomic features in a cohort with no known cardiovascular disease.[12] Test and retest images were acquired within an initial imaging session and participants returned for repeat test and retest image acquisitions during a second imaging session after two weeks. We calculated LV elasticity maps for each test and retest image to assess individual changes in passive LV stiffness utilizing patient specific geometry and boundary conditions to drive reconstructions of the biomechanical model. Because we are assessing within-subject test/retest variation within a short-acquisition window, there is no expectation of significant changes in subject cardiac stiffness between image acquisitions and allows for a direct test of potential method variability due to differences in geometry and boundary conditions or due to changes in image acquisitions. Reproducibility analysis is a necessary validation step for BIEM to determine the threshold of elasticity changes needed to distinguish biomechanical differences from methodological variation and to assess expected variability of LV elasticity in a control cohort.

2 Materials and Methods

2.1 *Patient Imaging Data*

In this reproducibility study, we assessed publicly available deidentified cardiac MR imaging data originally acquired for a reproducibility study of segmentation-based myocardial radiomic features.[12] The imaging cohort consisted of 10 participants, 7 women and 3 men with a mean age of 29 ± 13 years with no known cardiovascular disease developments during the study period. Each participant underwent test/retest cine cardiac MR imaging during an initial session (session 1) and returned for a follow-up session (session 2) two weeks later to undergo another set of test/retest imaging for a total of four cine images per participant. In each session, test/retest imaging consisted of an initial baseline image acquisition (test) followed by a subsequent cardiac MR image acquisition after a short break (retest). Cine balanced steady-state free precession short-axis cardiac MR images were acquired on a 3T Siemens scanner with an acquisition matrix of 208×229, with 25 time frames throughout the cardiac cycle with an approximate temporal resolution of 40 ms, repetition time/echo time $= 59/1.41$ ms, flip angle of 42 deg, in-plane resolution of 0.77 mm, and slice thickness of 8 mm. Two of the 10 available participant image sets were excluded from this study due to excessive cardiac motion blur artifact, leaving a total of 8 participants within the analysis cohort. To assess within-session reproducibility, initial test images were compared to retest images acquired within the same session for both imaging sessions 1 and 2 for a total of 16 comparisons. To assess between-session reproducibility, test images acquired during session 1 were compared to test images acquired during session 2, and retest images acquired during session 1 were compared to retest images acquired during session 2 for a total of 16 comparisons. As there is no evidence of cardiovascular disease during the study in this patient cohort, there is no expectation of significant LV elasticity change within-sessions or between-sessions.

2.2 *Image Processing*

Each cine cardiac MR image representing a complete cardiac cycle was analyzed using LV volume measurements to manually select time frames representative of passive diastole of the LV (after the opening of the mitral valve and before contraction of the left atrium). A midpoint time frame during passive diastole was automatically selected and used as a reference for a

nonrigid optical flow registration framework that registers each time frame to the midpoint time frame to estimate observed passive LV wall deformation through a diffeomorphic demons algorithm with a sigma value of 10 and 3 resolution levels.[13–15] Resulting deformation fields were smoothed using a 2D Gaussian smoothing function with a standard deviation of 4. The LV wall was segmented using AI-based segmentation software[16,17] and a finite-element mesh was generated based on LV segmentation with a nominal edge length of 0.75 mm. The mesh was then clustered into a total of 150 independent regions with average region patch size of 9 mm^2 using *k*-means clustering based on Euclidean distance for spatial modulus reconstruction. Estimated observed deformation was interpolated onto the finite-element mesh of the LV for iterative comparison to model-based deformation estimations for the inverse parameter estimation framework.[11]

2.3 *BEIM*

We previously developed a methodology for estimating spatial relative elasticity of the LV utilizing cine cardiac MR images acquired in the long-axis direction[11] for comparing cardiotoxic elasticity changes in a treatment cohort to a nontreatment comparator cohort.[18] In this study, we implement this model-based elasticity imaging methodology in a cohort with no indication of cardiovascular diseases with cine cardiac MR images acquired in the short-axis direction. This cardiac elasticity imaging methodology uses inherent motion of the LV during passive diastole to estimate LV elasticity. A schematic of the BEIM framework is shown in Fig. 1. While an abbreviated description follows, for further details, regarding the methodology the interested reader is referred to Ref. 11. In this work, we expanded upon our previous quasistatic model-based elasticity imaging framework based on mechanical equilibrium[19–22] for use on clinical cardiac MR images to generate 2D mechanical elasticity maps to characterize the LV. We assume in-plane anisotropic elasticity and out of plane isotropy assuming plane strain, whereby the strain in the z dimension is zero. Therefore, we calculate 2D anisotropic elasticity in-plane in the radial and circumferential direction for short-axis cardiac imaging acquisitions. LV finite-element mesh boundary conditions were extracted from observed deformation fields at the LV boundary. A linear transverse isotropic mechanical equilibrium equation [Eq. (1)] was solved over the LV finite-element mesh using the Galerkin method of weighted residuals based on extracted boundary conditions and an initial regional elasticity input [Eq. (2)]. To validate the ability of boundary conditions to drive our biomechanical model in the cardiac short-axis geometry, we performed an additional synthetic study with a known property distribution to examine the accuracy and stability of our method (see Supplementary Material). We assume a transversely anisotropic Hookean linear elastic material model that is described by Eq. (1). G is the material property of shear modulus, ν is the material property Poisson's ratio, and u is the displacement vector. To reduce degrees of freedom, Poisson's ratio was assumed as near-incompressible at 0.45 in both the circumferential and radial directions. This solution represented our model-estimated LV deformation during passive filling of the cardiac cycle. An objective-function defined

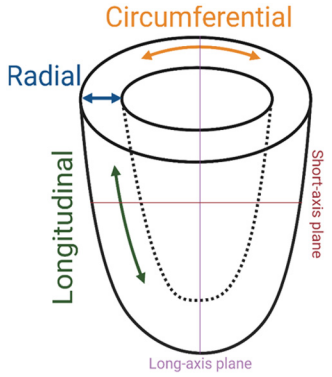

Fig. 1 Description of the short-axis and long-axis planes of the LV and definitions for stiffness in the radial and circumferential directions.

by the sum of squared error mismatch between the observed and model-estimated deformation fields was minimized using gradients calculated via the adjoint method.[23] The adjoint method was utilized to evaluate parameter sensitivity more efficiently than traditional finite difference methods.[24] A L-BFGS quasi-Newton algorithm[25,26] was used with the gradient information to iteratively update the modulus estimates in each region until overall error was minimized and a preset convergence tolerance was met (Fig. 2). The result is a model-based regional elasticity estimation of the LV. Relative mechanical elasticity was calculated in the x and y directions. Due to the heart's complicated geometry and fiber alignment, strain and cardiac elastography results are typically presented in a local cardiac-based coordinate system along the longitudinal, radial, and circumferential directions that form the natural axes of myocardial deformation;[27] however, these are not direct polar transforms of the Cartesian coordinate system, rather local directions along the LV that describe myocardial stiffness in reference to cardiac specific geometry. The resulting stiffness maps are then used to rotate to the circumferential and radial coordinate system in order to present the stiffness estimations in a coordinate system routinely adopted within the cardiac imaging research community to present cardiac motion (and strain) imaging metrics. To rotate between x/y stiffness and radial/transverse stiffness, an angle in degrees from

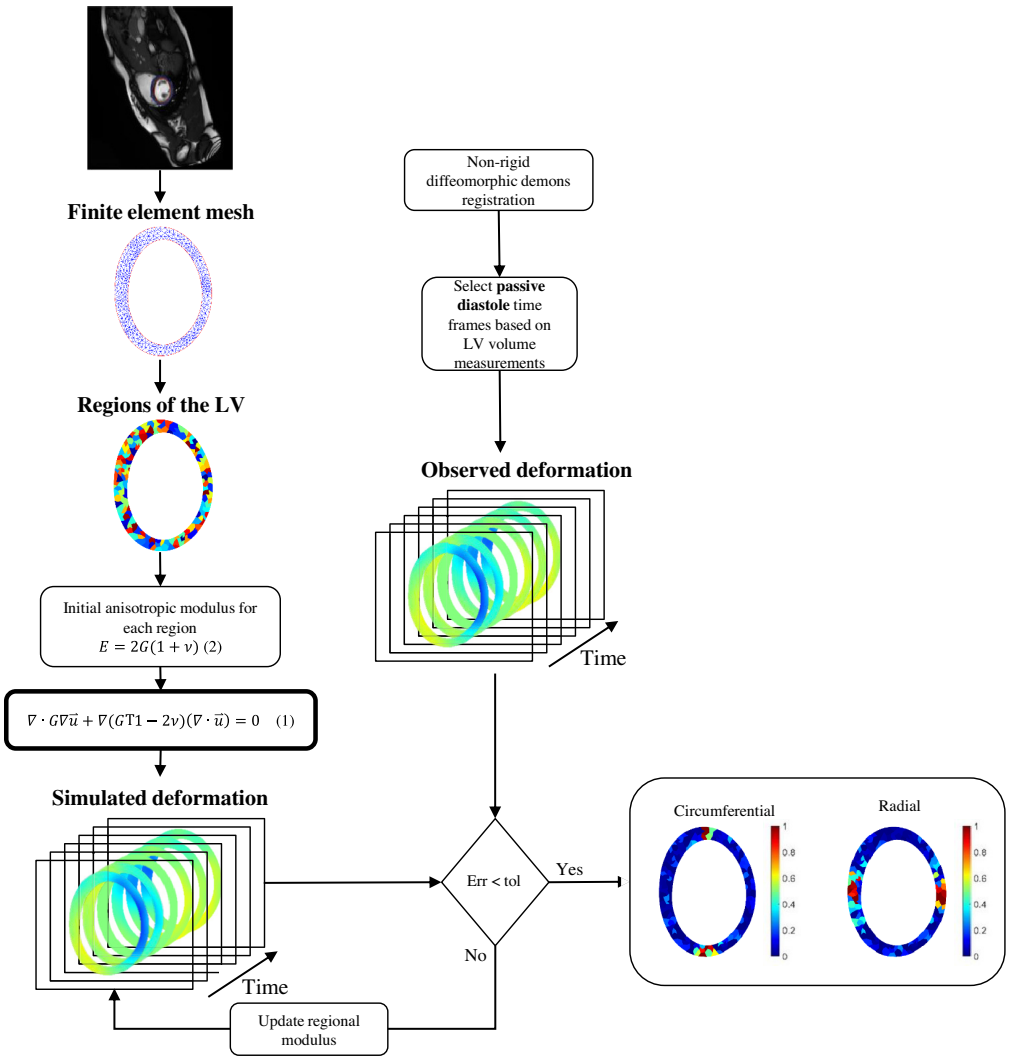

Fig. 2 Schematic of BEIM framework for LV elastic modulus inverse problem formulation. Model-calculated deformation solved over the LV finite-element mesh based on an initial assumption of elastic moduli is compared to observed deformation calculated from nonrigid registration. Region-based elastic modulus estimations were iteratively updated until a preset convergence tolerance is met. The result is a spatial elasticity map of the LV in the circumferential and radial axis directions.

0 to 360 is calculated from the center of each element to the center of the ventricle with a zero angle defined at the point between the septal segments (Fig. S1 in the Supplementary Material). A compliance matrix for each element is defined based on stiffness and assumed Poisson ratios. The compliance matrix is then rotated based on a stress and strain rotation matrix at each element, as in Ref. 28. Stiffness in the circumferential and radial directions is extracted from the resulting rotated compliance matrix at each element to obtain stiffness maps in the circumferential and radial directions, with directions represented in Fig. 1. Rotation matrix equations are listed in the Supplementary Material. Shear modulus maps were calculated based on the harmonic mean of circumferential and radial modulus axis directions, and a mechanical fractional mechanical stiffness anisotropy (FMSA) metric was calculated to describe the difference between the elasticity in the circumferential direction from the elasticity in the radial direction to give a metric of stiffness anisotropy within the LV. A value close to 1 indicates a large difference between circumferential and radial stiffness at that location and a value close to zero indicates similarity between circumferential and radial modulus to represent anisotropy of circumferential and radial moduli, indicative of erratic stiffness alignment [Eqs. (3) and (4)]. To compare elasticity maps across image acquisitions, in the previous work, we normalized estimated elasticity modulus maps by the median elasticity.[11] In this work, we improve this comparison by normalizing elasticity maps by the time-stress-integral[29] calculated over the endocardium based on the elasticity solution. This normalization factor is representative of the time resolved stress experienced by the endocardium throughout passive diastole and was calculated separately for each cardiac cine MR image acquisition. Normalization is required for direct comparison of elasticity maps across time points and patients due to the indeterminate nature of type 1 displacement-based boundary condition enforcement:

$$\nabla \cdot G\nabla\vec{u} + \nabla(G/1-2\nu)(\nabla \cdot \vec{u}) = 0, \tag{1}$$

$$E = 2G(1+\nu), \tag{2}$$

$$\mathrm{FMSA} = \frac{\sqrt{(E_{\mathrm{circ}} - E_{\mathrm{mean}})^2 + (E_{\mathrm{rad}} - E_{\mathrm{mean}})^2}}{\sqrt{E_{\mathrm{circ}}^2 + E_{\mathrm{rad}}^2}}, \tag{3}$$

$$E_{\mathrm{mean}} = \frac{E_{\mathrm{circ}} + E_{\mathrm{rad}}}{2}. \tag{4}$$

2.4 *Reproducibility Study*

Using BEIM, we estimated LV modulus maps for all test and retest image acquisition in both sessions 1 and 2. Estimated elasticity maps were divided into six anatomical segments[30] corresponding to the American Heart Association (AHA) LV model for short-axis midcavity slices,[31] shown in Fig. 3. Average normalized elasticity modulus was recorded within each segment and globally for the circumferential and radial axis directions, as well as average shear modulus and FMSA values for each cardiac MR image acquisition. As shown in Fig. 4, differences in elasticity solutions between each imaging test/retest set were then calculated for subsequent statistical reproducibility analysis. For within-session reproducibility analysis,

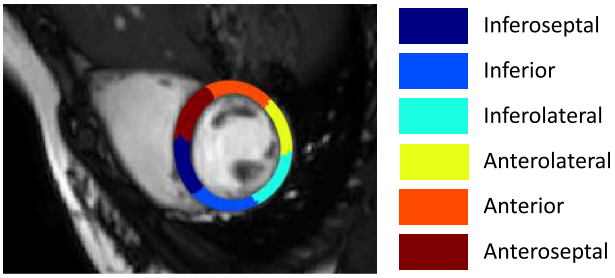

Fig. 3 LV segmentation based on the AHA model correlating to the short-axis midcavity segmentation diagram.[31]

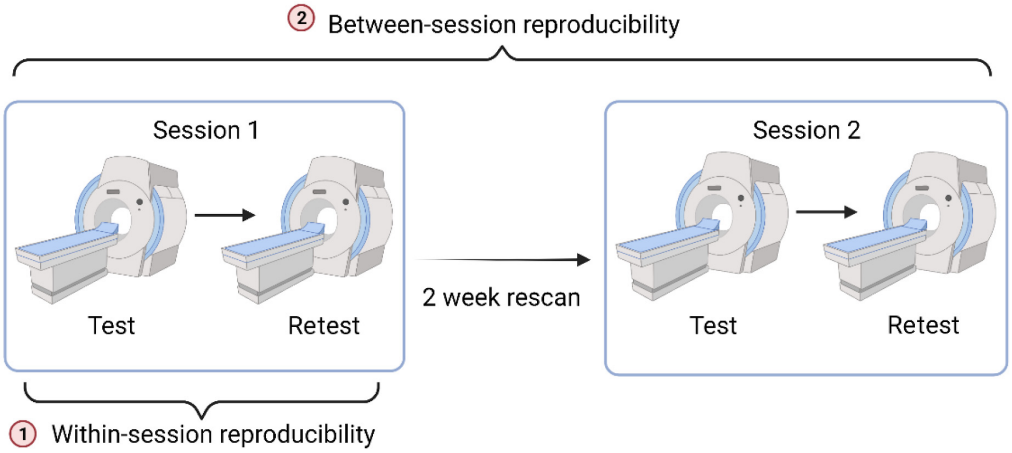

Fig. 4 Schematic of within-session and between-session reproducibility analysis.

differences between estimated LV modulus test maps and retest maps were calculated within both sessions 1 and 2. For between-session reproducibility analysis, differences between LV modulus test maps for session 1 and test maps for session 2 were assessed along with differences between LV modulus retest maps for session 1 and retest maps for session 2.

Reproducibility metrics were calculated for circumferential, radial, and shear modulus, and FMSA averages in each AHA segment and globally using Eqs. (5)–(9). The root-mean-square deviation (rMSD) and within subject standard deviation (wSD) were calculated based on differences in repeated measurements (d) with a total of n repeated measurements. Within-subject coefficient of variation (wCV) was calculated based on the overall mean of the parameter (μ) to estimate precision across metrics. A 95% confidence interval (CI) was calculated based on the standard deviation of the differences between repeated measurements to describe the range of expected variability within the cohort with the appropriate t-statistic for degrees of freedom, and a CI percent was calculated based on the average of each respective metric. The coefficient of repeatability (r) was also calculated to define the threshold for significance for an individual elasticity measurement using this methodology:

$$\mathrm{rMSD} = \sqrt{\frac{\Sigma d^2}{n}}, \tag{5}$$

$$\mathrm{wSD} = \frac{\mathrm{rMSD}}{\sqrt{2}}, \tag{6}$$

$$\mathrm{wCV} = \frac{\mathrm{wSD}}{\mu}, \tag{7}$$

$$95\%\ \mathrm{CI} = \pm\frac{\mathrm{tstat} * \mathrm{std}(d)}{\sqrt{n}}, \tag{8}$$

$$r = 2.77 * \mathrm{wSD}. \tag{9}$$

2.5 *Heart Rate Sensitivity Study*

Average heart rate was recorded during each image acquisition for each participant. Percent change in heart rate between test and retest images and between images acquired during sessions 1 and 2 were calculated to determine within and between-session heart rate variability. Percent change in heart rate was used to calculate repeatability, 95% CIs, and within subject coefficients of variation based on Eqs. (5)–(9).

2.6 *Segment Variability Study*

LV segmentations based on the AHA model for LV short-axis midcavity slices were designated by manually selecting a point on the LV at the midpoint of the right ventricle. The LV is then segmented into three equal anterior regions and three equal inferior regions based on the manual point selection. To assess variability due to AHA segment definitions, point selection was repeated six times for each participant in a blinded fashion to reduce observer familiarity. Average circumferential, radial, and shear modulus and FMSA measurements within each AHA segment for each repeated segmentation definition were calculated based on elasticity results from test images acquired during imaging session 1. Six repeated measurements of elasticity in each AHA segment for each participant were used to calculate repeatability, 95% CI, and within subject coefficient of variation based on Eqs. (5)–(9).

3 Results

3.1 *Reproducibility of Elasticity Maps*

Circumferential and radial mechanical elasticity maps were estimated using BEIM in a cohort of eight patients with no indication of cardiovascular disease. Shear modulus maps and FMSA values were calculated based on resultant elasticity maps. To assess within-session reproducibility, each elasticity metric for test images was compared with elasticity metrics for retest images within each imaging session (both sessions 1 and 2). To assess between-session reproducibility, test and retest images were compared between imaging sessions 1 and 2. Qualitatively, representative images show reasonable pattern repeatability both within- and between-session for circumferential, radial, and shear modulus as well as FMSA (Fig. 5).

3.2 *Reproducibility of Segmental and Global Elasticity*

To quantify statistical measures of reproducibility for calculated elasticity maps within and between sessions, average modulus (circumferential, radial, and shear) and FMSA were calculated. We calculated coefficients of repeatability to identify the threshold for significance for an individual patient measurement. 95% CIs were calculated to estimate the range of expected variability in a control cohort. wCV was calculated to compare metric precision. Each metric was

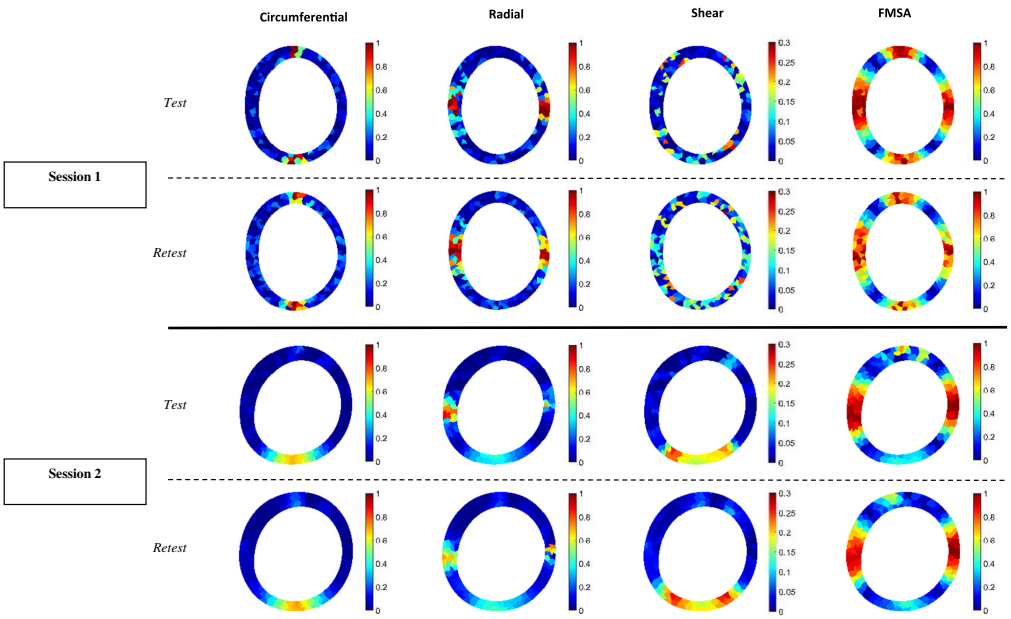

Fig. 5 Representative test/retest estimated modulus maps in the circumferential and radial axis dimension, shear modulus, and FMSA for sessions 1 and 2 image acquisitions of a single subject.

Table 1 Within-session and between-session reproducibility metrics for circumferential elasticity modulus in the inferoseptal, inferior, inferolateral, anterolateral, anterior, and anteroseptal AHA LV segments and global LV.

Within-session	Inferoseptal	Inferior	Inferolateral	Anterolateral	Anterior	Anteroseptal	Global
Repeatability	0.0865	0.167	0.228	0.223	0.327	0.165	0.108
±95% CI	0.0204 (28.0%)	0.0394 (22.5%)	0.0585 (20.6%)	0.0566 (26.4%)	0.0841 (33.7%)	0.0421 (43.7%)	0.0270 (14.9%)
wCV (%)	40.4	20.8	33.02	59.3	49.5	45.2	21.7
Between-session							
Repeatability	0.130	0.368	0.481	0.248	0.413	0.208	0.155
±95% CI	0.0235 (30.5%)	0.0830 (28.7%)	0.124 (49.7%)	0.0576 (42.4%)	0.104 (43.6%)	0.0471 (35.7%)	0.0389 (21.7%)
wCV (%)	61.0	46.0	69.7	66.0	62.5	57.0	31.1

Table 2 Within-session and between-session reproducibility metrics for radial elasticity modulus in the inferoseptal, inferior, inferolateral, anterolateral, anterior, and anteroseptal AHA LV segments and global LV.

Within-session	Inferoseptal	Inferior	Inferolateral	Anterolateral	Anterior	Anteroseptal	Global
Repeatability	0.303	0.173	0.195	0.367	0.224	0.217	0.134
±95% CI	0.0726 (26.4%)	0.0431 (13.6%)	0.0494 (23.5%)	0.0945 (41.6%)	0.0557 (35.3%)	0.0550 (32.0%)	0.0329 (15.0%)
wCV (%)	42.2	32.6	29.3	37.1	48.9	62.1	21.9
Between-session							
Repeatability	0.346	0.323	0.363	0.383	0.256	0.244	0.164
±95% CI	0.0766 (29.5%)	0.0775 (40.5%)	0.0937 (39.1%)	0.0982 (27.4%)	0.0632 (38.3%)	0.0572 (45.5%)	0.0409 (18.6%)
wCV (%)	48.1	61.1	54.7	38.7	56.1	69.9	26.9

Table 3 Within-session and between-session reproducibility metrics for shear modulus in the inferoseptal, inferior, inferolateral, anterolateral, anterior, and anteroseptal AHA LV segments and global LV.

Within-session	Inferoseptal	Inferior	Inferolateral	Anterolateral	Anterior	Anteroseptal	Global
Repeatability	0.0655	0.128	0.124	0.143	0.177	0.125	0.0780
±95% CI	0.0157 (29.3%)	0.0304 (22.6%)	0.0319 (23.6%)	0.0362 (40.0%)	0.0443 (32.8%)	0.0320 (44.2%)	0.0190 (19.1%)
wCV (%)	44.1	34.4	33.0	57.1	47.3	62.3	28.3
Between-session							
Repeatability	0.155	0.228	0.209	0.156	0.233	0.136	0.109
±95% CI	0.0317 (59.1%)	0.0529 (39.3%)	0.0532 (39.4%)	0.0382 (42.3%)	0.0576 (42.6%)	0.0287 (39.7%)	0.0267 (26.9%)
wCV (%)	105	61.1	55.6	62.2	62.2	67.9	39.6

Table 4 Within-session and between-session reproducibility metrics for mechanical FMSA in the inferoseptal, inferior, inferolateral, anterolateral, anterior, and anteroseptal AHA LV segments and global LV.

Within-session	Inferoseptal	Inferior	Inferolateral	Anterolateral	Anterior	Anteroseptal	Global
Repeatability	0.132	0.223	0.175	0.392	0.180	0.203	0.124
±95% CI	0.0341 (5.54%)	0.0564 (19.7%)	0.0451 (13.7%)	0.0918 (15.4%)	0.0463 (18.2%)	0.0523 (15.6%)	0.0318 (7.76%)
wCV (%)	7.73	28.1	19.2	23.7	25.5	21.8	10.9
Between-session							
Repeatability	0.432	0.383	0.456	0.382	0.317	0.401	0.205
±95% CI	0.111 (18.05%)	0.0984 (34.3%)	0.106 (32.2%)	0.0959 (16.0%)	0.0815 (32.0%)	0.0858 (25.6%)	0.0499 (12.2%)
wCV (%)	25.3	48.2	50.1	23.1	44.9	43.3	18.0

calculated within each LV segment and globally. Reproducibility statistics shown in Tables 1–4 indicated better global reproducibility than segment-based reproducibility. Global repeatability coefficients for estimated circumferential and radial modulus ranged from 0.164 to 0.108 and 95% CIs, and wCVs for global circumferential and radial modulus were <32%, shown in Tables 1 and 2. Additionally, for every metric, within-session results were more reproducible than between-session results.

Shear modulus maps were used to calculate shear reproducibility statistics, shown in Table 3. Global shear modulus reproducibility metrics remained consistent with circumferential and radial modulus reproducibility statics. Global repeatability coefficients for shear modulus were 0.0780 for within-session and 0.109 for between-session reproducibility. Global 95% CI and wCV were all below 40%.

Mechanical FMSA maps were calculated to indicate the degree of anisotropy between circumferential and radial modulus. FMSA maps exhibited good reproducibility (Table 4) with repeatability coefficients ranging from 0.124 to 0.456. All 95% CI percentages remained under 35%, and global CI was 7.76% for within-session and 12.2% for between-session FMSA comparisons. Global wCV was 10.9% for within-session and 18% for between-session FMSA comparison.

3.3 *Analysis of Elasticity Measurement Bias*

Bland–Altman plots of the difference between repeated measures versus the average of the measures for global circumferential and radial modulus for within-session measurements and between-session measurements were assessed to determine measurement bias and are shown in Fig. 6. Bland–Altman plots show no obvious bias in measurement.

3.4 *Heart Rate Sensitivity*

A heart rate sensitivity analysis was performed to quantify potential sources of variation related to simplifying model assumptions neglecting viscoelastic effects. Heart rate variability within the cohort was calculated based on percent differences in heart rate recorded during image acquisitions both within the same session and between sessions (Table 5). Within-session heart rate percent differences were −0.61% on average with a standard deviation of 5.2%, and between-session percent differences were 3.8% on average with a 16.1% standard deviation. Repeatability coefficients, 95% CIs, and wCVs were calculated and shown in Table 5. Results show minor to modest variability of heart rate during image acquisitions within the same session and between sessions.

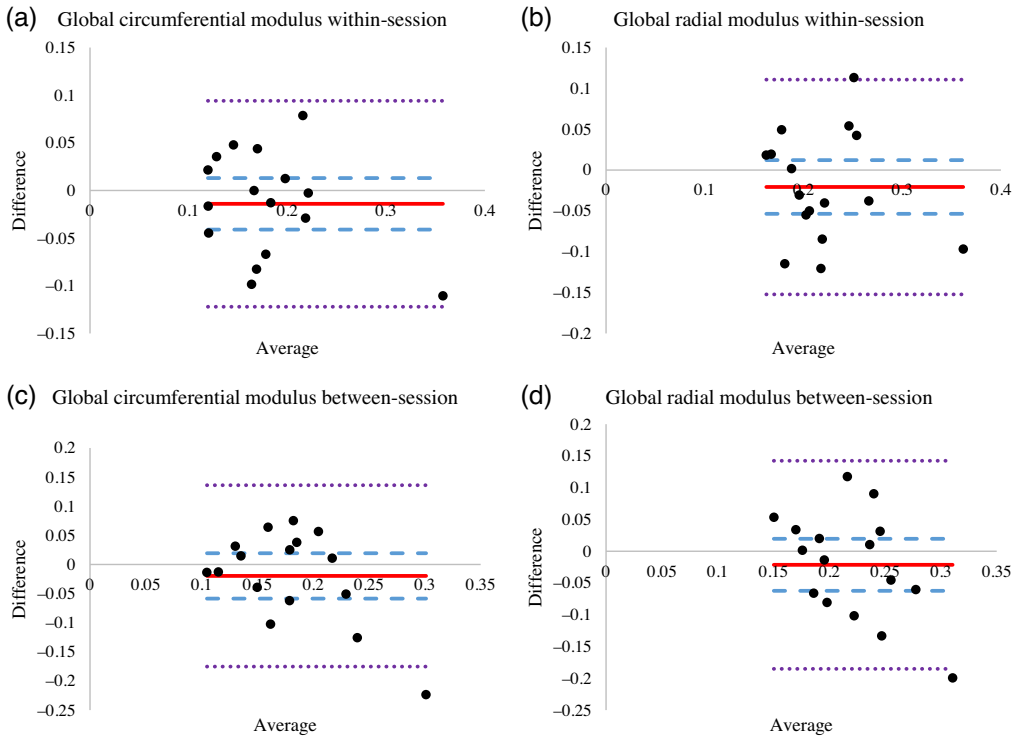

Fig. 6 Bland–Altman plots (difference versus average between each measurement) for global metrics for circumferential modulus (a) within-session and (c) between-session; radial modulus (b) within-session and (d) between-session. Mean difference is indicated by the red solid line, 95% CI is indicated by the blue dashed line, and Bland–Altman limits of agreement are indicated by the purple dotted line.

Table 5 Heart rate reproducibility statistics.

	Within-session		Between-session	
Avg. BPM (test/retest)	65.9 ± 9.6	64.9 ± 10.9	67.9 ± 15.8	68.0 ± 14.8
Repeatability	0.099		0.31	
±95% CI	0.025		0.79	
wCV	0.19		0.59	

3.5 *Segment Variability*

A segment variability analysis was performed to quantify the contributions of AHA segment definitions to overall variability. For subsequent reproducibility analysis, average elasticity metrics in each AHA segment were calculated based on six repeated segment definitions. Standard deviation and coefficient of variation were calculated for each participant and averaged within each segment to assess variability of elasticity measures due to AHA model segment definition and are shown in Table 6.

4 Discussion

In this study, we assessed the reproducibility of a BEIM for estimating mechanical stiffness of the LV myocardium. This methodology utilizes an inverse parameter estimation framework based on a linear transverse isotropic biomechanical model to estimate regional circumferential,

Table 6 Average standard deviation (Std Dev) and coefficient of variation (CoV) values for circumferential, radial, and shear modulus and FMSA measures for each segment definition ($n = 6$).

	Inferoseptal	Inferior	Inferolateral	Anterolateral	Anterior	Anteroseptal
Circumferential						
Std Dev	0.0090	0.022	0.019	0.00723	0.016	0.015
CoV (%)	6.54	6.75	7.01	4.08	9.33	10.0
Radial						
Std Dev	0.012	0.0068	0.010	0.0090	0.0059	0.0054
CoV (%)	3.82	2.79	5.32	2.29	4.93	4.10
Shear						
Std Dev	0.0035	0.0032	0.0045	0.0043	0.0042	0.0025
CoV (%)	6.13	1.84	3.17	4.89	4.91	3.18
FMSA						
Std Dev	0.012	0.013	0.0090	0.013	0.013	0.0081
CoV (%)	2.74	5.37	4.81	3.12	5.34	3.89

radial, and shear elastic moduli, which were used to calculate an FMSA metric based on 2D short-axis cardiac cine MR images. Results indicate moderate segment-based, and good global within-session and between-session reproducibility of LV modulus elasticity estimated using BEIM in a cohort of participants with no expected cardiovascular changes. Results specify thresholds for significance and overall methodological variability to facilitate implementing BEIM for assessing changes in LV stiffness to indicate cardiotoxicity due to breast cancer therapeutics.

We assessed differences in spatial mechanical elasticity maps between images acquired both within the same session and between images acquired in separate sessions two weeks apart in a cohort of patients with no expectation of significant changes in LV mechanical elasticity. Global elasticity measurements showed good reproducibility, comparable to cardiac strain measurement repeatability for CMR images acquired within the same session.[32] A previous study calculated reproducibility of LV clinical cardiac MR strain metrics utilizing feature tracking methods and found peak strain measurements had within-session coefficients of variation up to 20%, which is similar to our within session coefficient of variation of about 21% for global circumferential and radial modulus. Segment-based measurements are less repeatable than global measurements due to the variability in segment definitions per image acquisition, which is also demonstrated in strain analysis when comparing global to segment-based peak strain.[33] Our results showed expected increased within-session reproducibility of elasticity in all modulus axis directions and FMSA as compared to between-session reproducibility. Because modulus results are dependent on deformation fields estimated through nonrigid registration of cardiac cine MR images, greater differences in the underlying images lead to increased variation in the resulting deformation estimates that drive BEIM and therefore increased variability in resulting elasticity maps. Despite image differences and potential natural variation in cardiac stiffness between sessions, our results showed reasonable global reproducibility with coefficients of variation between ~21% and 31% and percent CI of ~15% to 22% for estimated circumferential and radial elastic modulus maps, which are reasonable ranges to be able to detect changes in diseased cohorts. In the previous work, data indicated a cohort of premenopausal women diagnosed with hormone receptor-positive breast cancer undergoing near-complete estrogen deprivation therapy exhibited short-term increases in global longitudinal and radial modulus values of ~40%, which was significantly greater than changes in elasticity in a comparator cohort of premenopausal patients. We also expect changes in stiffness due to anthracycline therapy to be larger with evidence

showing significant myocardial stiffness modulation due to chemotherapies,[34] indicating our methodology is capable of indicating changes in LV stiffness as a results of cardiotoxic antineoplastic therapies. Our results also define a threshold of significance to differentiate biological changes in modulus from methodological variability, important for potential future clinical implementation when assessing individual elasticity measurements. Bland–Altman plots demonstrate the absence of measurement bias, further validating the use of this methodology for assessing changes in elasticity and its potential for clinical implementation. Analyses were performed in a control cohort to establish reproducibility of BEIM in a cohort without significant changes in stiffness, but future work should include similar reproducibility assessments in a pathological cohort to establish reproducibility across a wider dynamic ranges of stiffness. Results indicated clinical feasibility of our methodology and reproducibility of metrics for defining LV stiffness changes needed to indicate true biomechanical differences from measurement variability.

Our method exhibits adequate reproducibility in a cohort of participants and has previously shown promise for identifying changes in mechanical stiffness due to cancer treatment-related cardiotoxicity but has several important limitations to be addressed in future studies. Results show reasonable reproducibility of global elasticity modulus and FMSA, comparable to ranges previously established for clinical cardiac strain imaging, but regional AHA segment-based metrics show reduced reproducibility. A similar phenomenon was demonstrated in the previous reproducibility studies when comparing segment-based strain measurements to global strain measurements.[33] Significant variation due to segment location selection variability and differences in LV shape between image acquisitions helps to explain these differences in degraded segment repeatability performance. In this study, segment locations are defined based on an initial point-based selection on the LV. Segment demarcations then create six equal segments that correspond to the AHA cardiac segmentation model. Variability in manual point selection introduces variation into the segment definitions and subsequent calculations of average segment modulus. Results shown in Table 6 indicate substantial variability that can be attributed to AHA segment definition location variability. Differences in LV size and shape between selected 2D midcavity slices due to patient motion and differences in slice alignment between test/retest image acquisitions also contributes to differences between image segmentations and is potentially exaggerated due to large slice thicknesses in acquired images. These results help to explain the phenomenon of decreased segment-based reproducibility when compared to global reproducibility. It is also important to note that BEIM provides spatial maps with significantly more spatial resolution to assess changes in mechanical elasticity within the ventricle as compared to traditional AHA segment definition averages, commonly used to assess cardiac strain measurements. Increased resolution of spatial elasticity analysis may be an important tool for assessing specific locations of changes in cardiac tissue mechanical characteristics. Another potential source of variation in our methodology is from the nonrigid registration-based estimate of observed deformation within the LV. BEIM uses image-based deformation estimations and uncertainty in registration would propagate to estimated stiffness. In this study, we utilize a diffeomorphic demons nonrigid image registration to estimate deformation of the LV during passive diastole. Previous studies have shown better reproducibility in cardiac mechanical modeling with such deformable registration techniques, as compared to feature tracking MRI,[35] however, the reproducibility of our method is dependent upon the accuracy of registration methods.

With respect to limitations to the underlying elasticity imaging methodology, our selected constitutive model assumes linear transverse isotropic elastic behavior with LV stiffness in two orthogonal geometric dimensions. This represents a simplification of cardiac mechanics, in which nonlinear viscoelastic anisotropy due to fiber alignment is a more refined assumption. This intentional parsimonious modeling approach was developed to utilize routine clinically relevant images to facilitate eventual clinical implementation and has shown sensitivity to changes in myocardial stiffness in the previous work.[11] As an initial step toward quantifying the impact of neglecting viscoelasticity, we assessed heart rate variability by calculating differences in heart rate for both within-session and between-session image acquisitions to assess a potential source of methodology variation. Heart rate variability was found to be minimal for within-session images and moderate for between-session images, representing a potential source of variability to address in future work. In this work, we sought to minimize variability due to

contributions from viscoelastic behavior by estimating elasticity maps using LV deformation during diastasis, a short-time frame during passive ventricular filling, in which ventricular pressure changes are negligible. However, in the future, our methodology could be expanded to include viscoelastic mechanical property reconstruction to account for variability in heart rate. In this work, we implement a two-dimensional (2D) stiffness reconstruction at the midslice of the LV. 2D models pose a methodological limitation due to inability to assess out-of-plane motion effects on stiffness estimates. We have chosen to estimate stiffness based on in-plane 2D deformations of the short-axis midanatomical slice of the LV to represent an average value of LV stiffness. In future studies, a similar method could be extended to assess 3D stiffness of the LV, but present work has focused on 2D estimations due to limitations from the relatively large thickness of routine clinical MR slices. Additionally, our current methodology allows for characterization of stiffness based on single-slice in-plane deformations that can be applied to any anatomical slice of the LV. In the present work, we focus on the midplane as a representative stiffness measurement due to the diffuse nature of cardiac fibrosis from antineoplastic therapies. Fibrotic infiltration from these mechanisms has been demonstrated to affect multiple cardiac planes,[36–39] and we have previously shown midslice estimations are capable of indicating significant changes in LV stiffness due to potential cardiotoxicities.[11] Another methodological limitation is due to the estimation of relative elastic modulus rather than absolute property reconstruction and subsequent lack of comparison to true mechanical stiffness of healthy myocardium. To decrease potential variation due to changes in median global stiffness, in this study, we normalized elasticity modulus maps relative to a previously developed time-stress-integral.[29] The time-stress-integral was calculated throughout passive diastole based on the elasticity solution such that the normalization factor scales with the indeterminate solution allowing elasticity solutions to be compared across image acquisitions. We also made an intentional simplifying assumption to enforce material stiffness in a geometric radial, circumferential, and longitudinal coordinate system rather that in alignment with myocardial fiber angles. The intended application is quantifying myocardial fibrosis due to cancer treatment-related cardiac damage, where the predominant mechanism for changes in cardiac stiffness is due to fibrotic collagen infiltration, rather than myocardial fiber-related mechanisms. Therefore, we choose to align stiffness directions with classically defined cardiac motion directions (longitudinal, radial, and circumferential shortening/elongation), as is routine with related cardiac strain-imaging measurements. Though additional follow-up studies are necessary to further interrogate the methodology, this study demonstrates a feasible and reproducible noninvasive BEIM for identifying biological changes in LV mechanical stiffness.

5 Conclusion

Previous studies indicate an important relationship between changes in myocardial stiffness and the onset of cardiovascular disease. As such, stiffness changes may represent a valuable early biomarker for cardiac degradation that has important implications in identifying and predicting cardiotoxicity. In the previous work, we developed and investigated a noninvasive BEIM for identifying changes in LV stiffness to indicate preclinical cardiotoxicity due to antineoplastic therapies.[11] This method employs a simple biomechanical model to estimate direct and functional spatial mechanical elasticity using clinically relevant cardiac MR imaging without the need for exogenous contrast agents or complex imaging sequences. In this study, we assessed the reproducibility of circumferential, radial, and shear modulus maps along with mechanical FMSA values in a publicly available imaging cohort of participants with no expectation of cardiovascular disease. Our methodology yielded reproducible results with comparable reproducibility metrics to cardiac strain imaging. Further, this study identified thresholds for classifying biological LV stiffness changes from methodological variation for subsequent clinical investigations. Our study demonstrates that BEIM can identify changes in LV stiffness with comparable reproducibility and key advantages to current methods of assessing cardiotoxicity. We demonstrate a clinically feasible strategy for assessing changes in LV elasticity and anisotropy to indicate preclinical cardiac degradation, which has applications in the cardio-oncology field to identify cardiotoxicity due to antineoplastic therapies in breast cancer patients as well as in cancer patients broadly.

Disclosures

Authors have no relevant financial interests in the manuscript and no other potential conflicts of interest to disclose.

Acknowledgments

This work was supported by the Williams Family Professorship in Breast Oncology and the National Institutes of Health-National Cancer Institute (Nos. K25CA204599 and P30CA012197).

References

1. D. A. Boyle, "Cancer and the broken heart: complications and implications of therapy-related cardiotoxicity," *J. Infusion Nurs.* **41**(4), 229–240 (2018).
2. F. Ades et al., "Cardiotoxicity of systemic agents used in breast cancer," *Breast* **23**(4), 317–328 (2014).
3. J. Doyle et al., "Chemotherapy and cardiotoxicity in older breast cancer patients: a population-based study," *J. Clin. Oncol.* **23**(34), 8597–8605 (2005).
4. K. L. Leonard and D. E. Wazer, "Cardiotoxicity associated with radiation for breast cancer," in *Toxicities of Radiation Treatment for Breast Cancer: Risks and Management Strategies*, J. L. Wright, ed., pp. 127–144, Springer International Publishing, Cham (2019).
5. S. Martel et al., "Breast cancer treatment-induced cardiotoxicity," *Expert Opin. Drug Saf.* **16**(9), 1021–1038 (2017).
6. S.-Y. Wang et al., "Cardiovascular events, early discontinuation of trastuzumab, and their impact on survival," *Breast Cancer Res. Treat.* **146**(2), 411–419 (2014).
7. I. Y. Gong et al., "Early diastolic strain rate measurements by cardiac MRI in breast cancer patients treated with trastuzumab: a longitudinal study," *Int. J. Cardiovasc. Imaging* **35**(4), 653–662 (2019).
8. A. Soufer and L. A. Baldassarre, "The role of cardiac magnetic resonance imaging to detect cardiac toxicity from cancer therapeutics," *Curr. Treat. Options Cardio Med.* **21**(6), 28 (2019).
9. T. J. Hall et al., "Recent results in nonlinear strain and modulus imaging," *Curr. Med. Imaging Rev.* **7**(4), 313–327 (2011).
10. M. M. Doyley, "Model-based elastography: a survey of approaches to the inverse elasticity problem," *Phys. Med. Biol.* **57**(3), R35–R73 (2012).
11. C. E. Miller et al., "Developing a biomechanical model-based elasticity imaging method for assessing hormone receptor positive breast cancer treatment-related myocardial stiffness changes," *J. Med. Imaging* **8**(5), 056002 (2021).
12. J. Jang et al., "Reproducibility of segmentation-based myocardial radiomic features with cardiac MRI," *Radiol.: Cardiothorac Imaging* **2**(3), e190216 (2020).
13. M. McCormick et al., "ITK: enabling reproducible research and open science," *Front. Neuroinf.* **8**, 13 (2014).
14. J.-P. Thirion, "Image matching as a diffusion process: an analogy with Maxwell's demons," *Med. Image Anal.* **2**(3), 243–260 (1998).
15. T. S. Yoo et al., "Engineering and algorithm design for an image processing API: a technical report on ITK—the Insight Toolkit," *Stud. Health Technol. Inf.* **85**, 586–592 (2002).
16. E. Heiberg et al., "Design and validation of segment—freely available software for cardiovascular image analysis," *BMC Med. Imaging* **10**, 1 (2010).
17. K. Berggren et al., "Multiple convolutional neural networks for robust myocardial segmentation," p. 4 (2020).
18. J. H. Jordan et al., "Myocardial function in premenopausal women treated with ovarian function suppression and an aromatase inhibitor," *JNCI Cancer Spectr.* **5**(4), pkab071 (2021).
19. R. H. Griesenauer et al., "Toward quantitative quasistatic elastography with a gravity-induced deformation source for image-guided breast surgery," *J. Med. Imaging* **5**(1), 015003 (2018).

20. R. H. Griesenauer et al., "Breast tissue stiffness estimation for surgical guidance using gravity-induced excitation," *Phys. Med. Biol.* **62**(12), 4756–4776 (2017).
21. J. A. Weis et al., "Assessing the accuracy and reproducibility of modality independent elastography in a murine model of breast cancer," *J. Med. Imaging* **2**(3), 036001 (2015).
22. J. A. Weis et al., "Development of a diaphragmatic motion-based elastography framework for assessment of liver stiffness," *Proc. SPIE* **9417**, 941703 (2015).
23. I. M. Navon, "Practical and theoretical aspects of adjoint parameter estimation and identifiability in meteorology and oceanography," *Dyn. Atmos. Oceans* **27**(1), 55–79 (1998).
24. A. A. Oberai, N. H. Gokhale, and G. R. Feijóo, "Solution of inverse problems in elasticity imaging using the adjoint method," *Inverse Probl.* **19**(2), 297–313 (2003).
25. D. C. Liu and J. Nocedal, "On the limited memory BFGS method for large scale optimization," *Math. Program.* **45**(1), 503–528 (1989).
26. J. Nocedal, "Updating quasi-Newton matrices with limited storage," *Math. Comp.* **35**(151), 773–782 (1980).
27. C. Ma, X. Wang, and T. Varghese, "Segmental analysis of cardiac short-axis views using Lagrangian radial and circumferential strain," *Ultrason. Imaging* **38**(6), 363–383 (2016).
28. J.-M. Zhao, X.-X. Song, and B. Liu, "Standardized compliance matrices for general anisotropic materials and a simple measure of anisotropy degree based on shear-extension coupling coefficient," *Int. J. Appl. Mech.* **8**(6), 1650076 (2016).
29. D.-W. Sohn et al., "LV peak instantaneous wall stress versus time-stress-integral as measures of afterload in aortic stenosis," *Heart* **101**(6), 478–483 (2015).
30. J. D'Errico, "Interparc," (2021). https://www.mathworks.com/matlabcentral/fileexchange/34874-interparc (accessed 4 December 2020).
31. M. D. Cerqueira et al., "Standardized myocardial segmentation and nomenclature for tomographic imaging of the heart," *Circulation* **105**(4), 539–542 (2002).
32. J. Lamy et al., "Scan-rescan reproducibility of ventricular and atrial MRI feature tracking strain," *Comput. Biol. Med.* **92**, 197–203 (2018).
33. J. Kar et al., "A validation of two-dimensional in vivo regional strain computed from displacement encoding with stimulated echoes (DENSE), in reference to tagged magnetic resonance imaging and studies in repeatability," *Ann. Biomed. Eng.* **42**(3), 541–554 (2014).
34. R. I. Mincu et al., "Left ventricular diastolic function following anthracycline-based chemotherapy in patients with breast cancer without previous cardiac disease-a meta-analysis," *J. Clin. Med.* **10**(17), 3890 (2021).
35. J. Wang et al., "Improved segmental myocardial strain reproducibility using deformable registration algorithms compared with feature tracking cardiac MRI and speckle tracking echocardiography," *J. Magn. Reson. Imaging* **48**(2), 404–414 (2018).
36. A. M. Varnava et al., "Hypertrophic cardiomyopathy: the interrelation of disarray, fibrosis, and small vessel disease," *Heart* **84**(5), 476–482 (2000).
37. E. B. Tham et al., "Diffuse myocardial fibrosis by T1-mapping in children with subclinical anthracycline cardiotoxicity: relationship to exercise capacity, cumulative dose and remodeling," *J. Cardiovasc. Magn. Reson.* **15**, 48 (2013).
38. L. Elbl, H. Hrstkova, and V. Chaloupka, "The late consequences of anthracycline treatment on left ventricular function after treatment for childhood cancer," *Eur. J. Pediatr.* **162**(10), 690–696 (2003).
39. H.-M. Chang et al., "Cardiovascular complications of cancer therapy: best practices in diagnosis, prevention, and management: part 1," *J. Am. Coll. Cardiol.* **70**(20), 2536–2551 (2017).

Biographies of the authors are not available.